A Comparison of Depth-Dependent Microstructures of Ion-Irradiated 316- Type Stainless Steels

R.L. Sindelar, R.A. Dodd and G.L. Kulcinski

June 1984

UWFDM-583

Presented at the 12th Intern. Symposium on the Effects of Radiation on Materials, Williamsburg, VA, June 18-20, 1984.

FUSION TECHNOLOGY INSTITUTE

UNIVERSITY OF WISCONSIN

MADISON WISCONSIN

A Comparison of Depth-Dependent Microstructures of Ion-Irradiated 316- Type Stainless Steels

R.L. Sindelar, R.A. Dodd and G.L. Kulcinski

Fusion Technology Institute
University of Wisconsin
1500 Engineering Drive
Madison, WI 53706

http://fti.neep.wisc.edu

June 1984

UWFDM-583

Presented at the 12th Intern. Symposium on the Effects of Radiation on Materials, Williamsburg, VA, June 18-20, 1984.

A COMPARISON OF DEPTH-DEPENDENT MICROSTRUCTURES OF ION-IRRADIATED 316-TYPE STAINLESS STEELS

R.L. Sindelar, R.A. Dodd and G.L. Kulcinski

Fusion Engineering Program
Nuclear Engineering Department
University of Wisconsin-Madison
Madison, WI 53706

June 1984

UWFDM-583

Introduction

Materials to be used in the construction of near-term fusion reactors will be tailored to meet various criteria. These criteria include the maintenance of mechanical stability and the resistance to cavity-induced swelling during exposure to intense radiation environments. Even minimal variations in the composition of a promising alloy may lead to different microstructural/microchemical evolutions under irradiation which cause the alloy to not satisfy the design requirements [1,2].

Slight compositional alterations of major alloying elements and even "impurity" elements in 316-type stainless steels have produced varied irradiation responses. This behavior has been observed after fast reactor [3,4], high-energy electron [5], and heavy-ion [6,7] radiation exposure. In addition, reactive (e.g. hydrogen and oxygen) gases dissolved in a metal seem likely to assist in cavity nucleation and growth processes [8-10]. Therefore, actual large scale fabrication of reactor components may have to be monitored carefully to assure the "proper" composition of the finished product.

One type of 316 stainless steel with reduced impurity levels has been recently studied in dual-ion and fast reactor experiments [11-17]. This alloy, P7, was fabricated as a "pure" 316 stainless steel alloy in order to provide an alloy resistant to phase instabilities. This alloy was found to swell readily with essentially no incubation dose. This paper investigates the different response of this "pure" 316 stainless steel alloy, P7, compared to the MFE heat of 316 stainless steel after 14-MeV Ni-ion irradiation.

Experimental

The compositions of the alloys irradiated in this study are shown in Table 1. Note that the MFE heat #15893 of 316 SS contains higher levels of most impurity elements than does P7. Also note that the P7 alloy stock contains a high matrix oxygen content. The pre-irradiation treatment of the P7 alloy stock involved rolling to a thickness of 500 μm followed by a solution quench after a 1 hour anneal in air at 1000°C. Oxygen was present in the anneal furnace as evidenced by a surface oxide coating on the P7 alloy, and this had to be removed prior to irradiation. A simple calculation using oxygen solubility data [18,19] estimates that the resultant matrix is saturated with oxygen at or near the value shown in Table 1. Pre-irradiation preparation consisted simply of successive mechanical polishing operations using abrasives down to 0.3 μm alumina powder. The samples were not electropolished prior to irradiation in order to preclude the introduction of hydrogen into the specimen [20]. Irradiations were performed at the University of Wisconsin Heavy-Ion Irradiation Facility using 14 MeV Ni^{3+} ions.

Figure 1 shows the displacement damage as a function of depth for 14 MeV Ni ions on 316-type stainless steel targets. Recent studies [22] have found that the displacement efficiency (K) varies as a function of PKA energy, in contrast to the standard value of K = 0.8 as proposed by Torrens and Robinson [23]. At high energies the value of K has been found to be about 0.3, independent of energy. Therefore, we have used K = 0.3 in all of our dpa calculations in this paper.

The samples were irradiated at temperatures between 500°C and 650°C (0.45 - 0.55 T_m) to peak damage levels of 20 dpa (K = 0.3). Table 2 lists the irradiation parameters used in this study. Post-irradiation preparation for

TEM analysis involved a cross-section technique described in detail elsewhere [24]. This procedure allows the entire damage range shown in Fig. 1 to be analyzed for a single irradiated sample. The microscopy analysis was performed using a JEOL TEMSCAN-200 CX electron microscope.

Voids densities were determined in 0.25 μm intervals along the ion range with the data points plotted in the middle of the interval. Error bars reflect the uncertainty in foil thickness determination (~ 10%) and the statistical counting uncertainty ($\sqrt{n}/n$) where n is the total number of voids in a 0.25 μm interval.

Results

Figure 2 shows the TEM micrographs which span the entire damage range of the low (5 dpa peak, K = 0.3) and high fluence (20 dpa peak, K = 0.3) 500°C irradiation of the P7 alloy. Figure 3 shows the average cavity diameter, cavity density, and cavity-induced swelling as a function of distance from the sample surface for these two irradiation conditions. It is evident from Fig. 3 that there is a suppression in the average cavity diameter and number density of the high fluence specimen in a region approximately 2.0 to 2.6 μm from the sample surface. This region is coincident with the range of the bombarding Ni ions. The suppression of cavity growth [25] and cavity nucleation [26,27] is thought to be caused by these injected ions providing interstitials in excess of the Frenkel defects produced during the irradiation.

Figure 4 contains the through-range microstructures of the low (5 dpa peak, K = 0.3) and high fluence (20 dpa peak, K = 0.3) 650°C irradiation of the P7 alloy. Figure 5 shows the average cavity diameter, cavity density, and cavity-induced swelling as a function of distance from the sample surface for these two irradiation conditions. It is apparent that there is bi-modal void

distribution in the peak damage region (see Fig. 1) at 650°C. To aid in distinguishing the two distributions, cavities > 100 nm were classified as "large voids" whereas those < 100 nm were labeled "small voids." The diameters of the "large voids" in the high fluence specimen approach the value of the TEM specimen thickness in this region (~ 200 nm). Hence, many of these voids intersect the foil surface. Stereo microscopy analysis in thicker regions of the foil revealed that these features are not artifacts but are completely contained within the specimen. Figure 4 and 5 suggest that the voids present at the low fluence are the precursor distribution of the "large void" distribution in the high fluence sample. A denuded zone of ~ 0.6 μm from the foil surface is present in the high fluence 650°C sample. The absence of voids in this region is attributed to the diffusion of defects to the free surface. Garner and Thomas [28] have shown in HVEM studies that a 0.6 μm void free zone also exists at a dose of 6 dpa (K = 0.8) in 316 SS at 650°C.

Figure 6 shows the precipitation response of the entire ion-damage region for the 316 SS sample. It is evident that there is an absence of cavities throughout the entire damage region. In addition, the irradiation produced a network dislocation structure whose density is ~ 10^{10} cm^{-2} throughout the damage region.

The precipitation response of this sample to irradiation can be seen in the optical micrographs of Fig. 7. The ~ 3 μm of enhanced precipitation at the interface corresponds to the depth of the damage region characteristic of 14 MeV Ni ions. The precipitation response in the damage region was predominantly needle-shaped precipitates. These precipitates had a uniform distribution over the depth of ~ 0.75 μm to ~ 3.0 μm with an average length of 150 nm and density ~ 1 x 10^{14} cm^{-3}. Figure 7d displays a micrograph of the damage

region which shows these precipitates at a depth of 1.5 μm from the foil surface. Needle-shaped precipitates of this approximate size and density have previously been observed in dual-iron irradiation studies [29] where they were determined to be an iron phosphide phase, Fe_2P. The typical composition of the needles given was (wt.%) 16Si-5P-4S-19Cr-29Fe-27Ni.

Optical micrographs of the cross-sectioned sample (Figs. 7a,7b) reveal extensive grain boundary precipitation throughout the unirradiated region. TEM analysis shows that these regions contain blocky $M_{23}C_6$ precipitates (see Fig. 7c) along the grain boundaries. Figure 7b also includes a feature in the boundary region where two austenite grains have intersected at the nickel plate - 316 SS foil interface. This is an artifact of the plating process. Corrosion at this location occurred when the irradiated foil was anodic in the strike cell [24]. When the current was reversed this corrosion pit was filled with the nickel plate.

Discussion

The above results show a varied response to 14-MeV Ni-ion irradiation for i) identical samples irradiated at different temperatures and for ii) samples with different impurity and reactive gas levels irradiated at the same temperature. The response of each set of samples to heavy-ion irradiation showed interesting microstructural features.

First, a suppression in cavity number density and average diameter was noted at the region that coincides with the range of the incident ion species in the high fluence 500°C P7 sample. A retardation of cavity growth from these injected interstitials has been previously postulated by Brailsford and Mansur [25]. The suppressed cavity density is attributed to a decreased cavity nucleation rate in this region where the bombarding ions come to

rest. This effect is important at temperatures where recombination is the dominant loss mechanism for point defects, and is well modelled elsewhere [27]. A discrepancy does exist, however, in the low fluence 500°C P7 sample where no dip in the cavity density is noted at the peak damage region. In addition, the dpa level at 1 μm in the high fluence sample was approximately the same as the peak dpa value of the low fluence sample (5 dpa), yet the cavity number density was slightly greater in the peak damage region of the low fluence sample (see Fig, 3). This result may be attributed to the difficulty in distinguishing small cavities (1 nm - 2 nm) from artifacts in a TEM foil ~ 100 nm thick and therefore the discrepancy lies within the error estimation of the cavity number density.

In the 650°C irradiations of the P7 alloy, a bi-modal void distribution was observed to evolve. A bi-modal void distribution has only been previously observed in a heavy-ion irradiated single phase material when it contained injected or transmuted gas. The presence of a high matrix oxygen level, which is assumed to be highly mobile in the P7 matrix at this 650°C irradiation temperature, is believed to be responsible for this bi-modal void development. Calculations using oxygen solubility data from Fromm and Gebhardt [18], the heat of chemisorption equations of Tanaka and Tamaru [30], and the heat of oxide formation from Robie et al. [31], predict that the heat of chemisorption of oxygen on γ-Fe (-272 kJ/mole oxygen at 650°C) is greater than the heat of solution of oxygen in γ-Fe (-93 kJ/mole oxygen at 650°C). This large difference provides the driving force for oxygen to come out of solution and collect on a clean, free surface. Oxygen should therefore be attracted to the surface of a void nucleus, and thus affect the surface energy of the cavity. According to Bernard and Lupis [32], the surface energy γ is determined by

$$\gamma = \gamma_o + \frac{kT}{A} \ln (1-\Theta)$$

where Θ is the degree of coverage of the surface, γ_o is the energy of the clean metal surface ($\Theta = 0$) and A is the area effectively occupied by a chemisorbed oxygen atom. Jones and Wolfer [33] recently performed a similar analysis of hydrogen in α-iron with a resultant substantial reduction in surface energy. When surface energy is reduced, void nuclei are more readily stabilized and accelerated cavity growth can take place.

The void nucleation rate in P7 should be the greatest in the peak displacement rate region (2.3 μm depth) as shown by another study [27]. Using a diffusion equation given for oxygen in γ-iron given in [38],

$$D = 5.75 \exp \left(\frac{-40,300}{1.98\ T}\right) \text{ cm}^2/\text{s}$$

it can be shown that $D = 1.5 \times 10^{-9}$ cm^2/s at 650°C. Thus, oxygen should be highly mobile and may freely migrate towards the void embryos forming in the peak damage region. This process appears to be efficient in reducing the surrounding matrix oxygen level since the low fluence 650°C P7 sample contains voids in the peak damage region only. Later in the irradiation, additional cavities can nucleate and grow throughout the damage region. Those cavities in the peak region have a lower number density and average diameter which could be due to the effect of the "large voids." Note, however, the difference in the cavity number density of the low fluence sample and the "large void" density in the high fluence sample. A calculation of the maximum possible density of 200 nm spheres is ~ 1×10^{14}/cm^3 when considering a simple cubic dense packing arrangement. A more realistic estimate would take a

simple cubic arrangement of spheres with spacing equal to one diameter. This would yield a density ~ 2 x 10^{13} spheres/cm^3. Therefore, since the measured void density is ~ 4 x 10^{14} cavities/cm^3 in the low fluence sample, an interactive process must take place between the cavities during their growth stage in order to reduce their number density to the ~ 2 x 10^{13} cavities/cm^3 observed for the large size class in the high fluence sample. One possible process to reduce void number density in this manner would be the actual coalescence of voids. Mansur [34] describes such a process and cites experimental evidence for its occurrence.

Lastly, the needle-shaped precipitation which occurred in the damage region only for the 650°C 316 SS sample in this study is similar to that observed in dual ion-irradiation studies [29,35,36]. This phase appeared early in these irradiations only to dissolve upon further irradiation. Recently, Lee et al., discovered these needles after dual-ion irradiation of an alloy similar to 316 SS and identified them as the Fe_2P phase.

No thermal aging studies of 316 SS have shown the Fe_2P phase to form. However, such a phase has formed in 321 SS [37]. In the Lee et al. study [29], a post-irradiation thermal aging at the irradiation temperature of 675°C for 16 hours was seen to cause a partial dissolution of the Fe_2P phase. In the present study, a TEM foil having the needle precipitates was ion-milled without specimen cooling. Subsequent TEM analysis of this post-milled sample revealed that no needles were present. The tentative conclusions of these experimental observations suggest that the needle-shaped Fe_2P phase is radiation-induced and will dissolve at high temperatures in the absence of irradiation. Further work is necessary to confirm this hypothesis.

Conclusions

The cross-section technique has been applied to heavy-ion irradiated 316-type stainless steels to allow the complete damage region to be analyzed. Several interesting effects of the ion damage were noted:

1. Suppression in void nucleation and growth was observed in a region near the end of range of the incident ions in the low temperature (500°C) irradiation of the P7 alloy. This suppression is attributed to the "excess interstitial" effect of the bombarding ions.
2. A bi-modal void distribution was observed to evolve in the peak damage region of the high temperature (650°C) irradiation of the P7 alloy. Oxygen initially present in the matrix is believed to be responsible for this development.
3. Needle-like precipitates were found in the damage region of heavy-ion irradiated 316 SS. This phase has been observed before as a transitory phase in dual-ion irradiation studies where it was identified as an Fe_2P phase.

Acknowledgements

The authors wish to express thanks to L.E. Seitzman for his assistance in this project. This research was sponsored by the Department of Energy.

References

[1] Kulcinski, G.L., "Materials Problems and Possible Solutions for Near Term Tokamak Fusion Reactors," Proceedings of the International School of Fusion Reactor Technology, Meeting on Tokamak Reactors for Breakeven - A Critical Study of the Near-Term Fusion Reactor Programme, held at Erice, Sicily, Sept. 20 - Oct. 1, 1976.

[2] Abdou, M.A. and El-Derini, Z., J. Nucl. Mat. 85 & 86 (1979) 57-64.

[3] Bates, J.F. and Johnston, "Effects of Alloy Composition on Void Swelling," International Conference: Radiation Effects in Breeder Reactor Structural Materials, AIME (1977) pp. 625-644.

[4] Weiner, R.A. and Boltax, A., "Comparison of High-Fluence Swelling Behavior of Austenitic Stainless Steels," Effects of Radiation on Materials: Tenth Conference, ASTM STP 725, 1981 pp. 484-499.

[5] Nakata, K., et al., "Effects of Nitrogen and Carbon on Void Swelling in Electron-Irradiated Austenitic Stainless Steel," Third Topical Meeting on Fusion Reactor Materials, Albuquerque, NM, Sept. 19-23, 1983.

[6] Williams, T.M., J. Nucl. Mat. 88 (1980) 217.

[7] Bates, J.F., et al., "Radiation of Irradiation-Induced Creep and Swelling in AISI 316 by Compositional Modifications," Effects of Radiation on Materials, ASTM STP 725 (1981) p. 73.

[8] Farrell, K., Rad. Effects Vol. 53 (1980) 175-194.

[9] Glowinski, L.D. and Fiche, C., J. Nucl. Mat. 61 (1976) 22; 61 (1976) 29.

[10] Wolfer, W.G., "Advances in Void Swelling and Helium Bubble Physics," Third Topical Meeting on Fusion Reactor Materials, Albuquerque, NM, Sept. 19-23, 1983.

[11] Farrell, K. and Packan, N.H., J. Nucl. Mat. 85 & 86 (1979) 683-687.

[12] Packan, N.H. and Farrell, K., J. Nucl. Mat. 85 & 86 (1979) 677-681.

[13] Miyahara, K., et al., Effects of Radiation on Materials: Eleventh Conference, ASTM STP 782 (1982) 941-952.

[14] Packan, N.H., J. Nucl. Mat. 103 & 104 (1981) 1029.

[15] Johnston, W.G., et al., "The Effect of Metallurgical Variables on Void Swelling," General Electric Report 76CRD010, Jan. 1976.

[16] Leitnaker, J.M., et al., J. Nucl. Mat. 49 (1973) 57-66.

[17] Brager, H.R. and Garner, F.A., Effects of Radiation on Materials: Eleventh Conference, ASTM STP 782 (1982) 152-165.

[18] Fromm, E. and Gebhardt, E., "Gase and Kohlenstoff in Metallen," Reine und angewandte Metallkunde in Einseldarstellungen, Band 26, Springer-Verlag, 1976.

[19] Coplan, D. and Burr, A.A. Trans. AIME 203 (1955) 1052.

[20] Whitley, J.B., Ph.D Thesis, University of Wisconsin, 1978.

[21] Brice, D.K., "Ion Implantation Range and Energy Deposition Codes COREL, RASE4, and DAMG2," SAND 77-0622 (1977).

[22] Kinney, J.H., et al., Presented at the Third Topical Meeting on Fusion Reactor Materials, Albuquerque, NM, Sept. 19-23, 1983.

[23] Torrens, I.M. and Robinson, M.T., Radiation Induced Voids in Metals, J.W. Corbett and I.C. Ianniello, eds. (1972) 739.

[24] Sindelar, R.L., et al., Presented at the Third Topical Meeting on Fusion Reactor Materials, Albuquerque, NM, Sept. 19-23, 1983.

[25] Brailsford, A.D. and Mansur, L.K., J. Nucl. Mat. 71 (1977) 110.

[26] Plumton, D.L. and Wolfer, W.G., J. Nucl. Mat. 120 (1984)

[27] B. Badger Jr., et al., "Experimental Investigation of the Effect of Injected Interstitials on Void Formation," 12th International Symposium on the Effects of Radiation on Materials, 18-20 June 1984, Williamsburg, VA.

[28] Garner, F.A. and Thomas, L.E., Effects of Radiation on Substructure and Mechanical Properties of Metals and Alloys, ASTM STP 529 (1973) 303-325.

[29] Lee, E.H. et al., "The Effect of Phosphorus on the Swelling and Precipitation Behavior of Austenitic Stainless Steels During Irradiation," Third Topical Meeting on Fusion Reactor Materials, Albuquerque, NM, Sept. 19-23, 1983.

[30] Tanaka, K. and Tamaru, K., J. of Catalysis 2 (1963) 366.

[31] Robie, R.A., et al., Thermodynamic Properties of Minerals and Related Substances at 298.15 K and 1 Bar (10^5 Pascals) Pressure and at Higher Temperatures, U.S. Government Printing Office, Washington, 1978.

[32] Bernard, G. and Lupis, C.M.P., Surface Science 42 (1974) 61-85.

[33] Jones, R. H. and Wolfer, W.G., Third Topical Meeting on Fusion Reactor Materials, Albuquerque, NM, Sept. 19-23, 1983.

[34] Mansur, L.K., Nuclear Technology 40 (1978] pp. 5-34.

[35] Packan, N.H. and Farrell, K., Effects of Radiation on Materials: Eleventh Conference, ASTM STP 782, (1982) pp. 885-894.

[36] Wood, S., et al., Effects of Radiation on Materials: Tenth Conference, ASTM STP 725 (1981) pp. 455-469.

[37] Bentley, J. and Leitnaker, J.M., The Metal Science of Stainless Steels, Proceedings of Symposium on the 107th AIME Annual Meeting (1978), Eds. E.W. Collings and H.W. King, The Metallurgical Society of AIME, pp. 70-91.

[38] Swisher, J.H. and Turkdogan, E.T., Trans. Met. Soc. AIME 239 (1967) 426-431.

Table 1. Composition of MFE Heat # 15893 316 SS and the "Pure" 316 SS, P-7 Alloy

	Composition (wt.%)					
Material	Cr	Ni	Mo	Mn	Si	C
316 SS	17.4	12.6	2.2	1.81	0.65	0.05
P7 alloy	17	16.7	2.5	0.03	0.1	0.005

Material	P	S	Ti	O	W	Fe
316 SS	0.030	0.020	< 0.001	0.005	-	Bal.
P7 alloy	-	-	0.01	0.03	0.068	Bal.

Table 2. 14 MeV Ni-Ion Irradiation Parameters

Samples irradiated at a flux of 3×10^{11} ions/cm^2/s.

Material	dpa at 1 μm*	peak dpa*	Fluence (ions/cm^2)	Irradiation Temp. (°C)
P7 alloy	1	5	0.8×10^{16}	500
P7 alloy	4	20	3.3×10^{16}	500
P7 alloy	1	5	0.8×10^{16}	650
P7 alloy	4	20	3.3×10^{16}	650
316 SS	4	20	3.3×10^{16}	650

*displacement efficiency K = 0.3

Figure Captions

Fig. 1. Damage (dpa) vs. distance from the irradiated surface calculated using the Brice code [21]. The damage efficiency (K) used is 0.3. E_d = 32 eV.

Fig. 2. TEM micrographs spanning the entire damage region for the low and high fluence 500°C irradiations of P7. Note the suppression in cavity density and average diameter at the ~ 2.5 μm depth in the high fluence sample.

Fig. 3. Cavity mean size, density, and swelling results for the low and high fluence 500°C irradiation of P7.

Fig. 4. TEM micrographs spanning the entire damage region for the low and high fluence 650°C irradiations of P7. Note the evolution of a bi-modal void distribution near the damage peak at ~ 2.5 μm.

Fig. 5. Cavity mean size, density, and swelling results for the low and high fluence 650°C irradiation of P7.

Fig. 6. TEM micrographs spanning the entire damage region for the 316 SS sample. Note the absence of voids and the residual absorption contract of the needle-like phase in the low contrast micrographs.

Fig. 7. a), b) Optical micrographs for the 650°C 316 SS sample. The highly etched region on the nickel plate - 316 SS foil interface (vertical band on left hand side of micrograph) is clearly visible. This ~ 3.0 μm width region corresponds with TEM observations of needle-like precipitates which are found up to ~ 3.0 μm from the foil surface.
c) TEM micrograph of $M_{23}C_6$ precipitates on a grain boundary in the unirradiated region. This precipitation is evident in Fig. 7a.
d) TEM micrograph of the needle-like precipitates in a region ~ 1.5 μm from the foil surface.

FIGURE 1

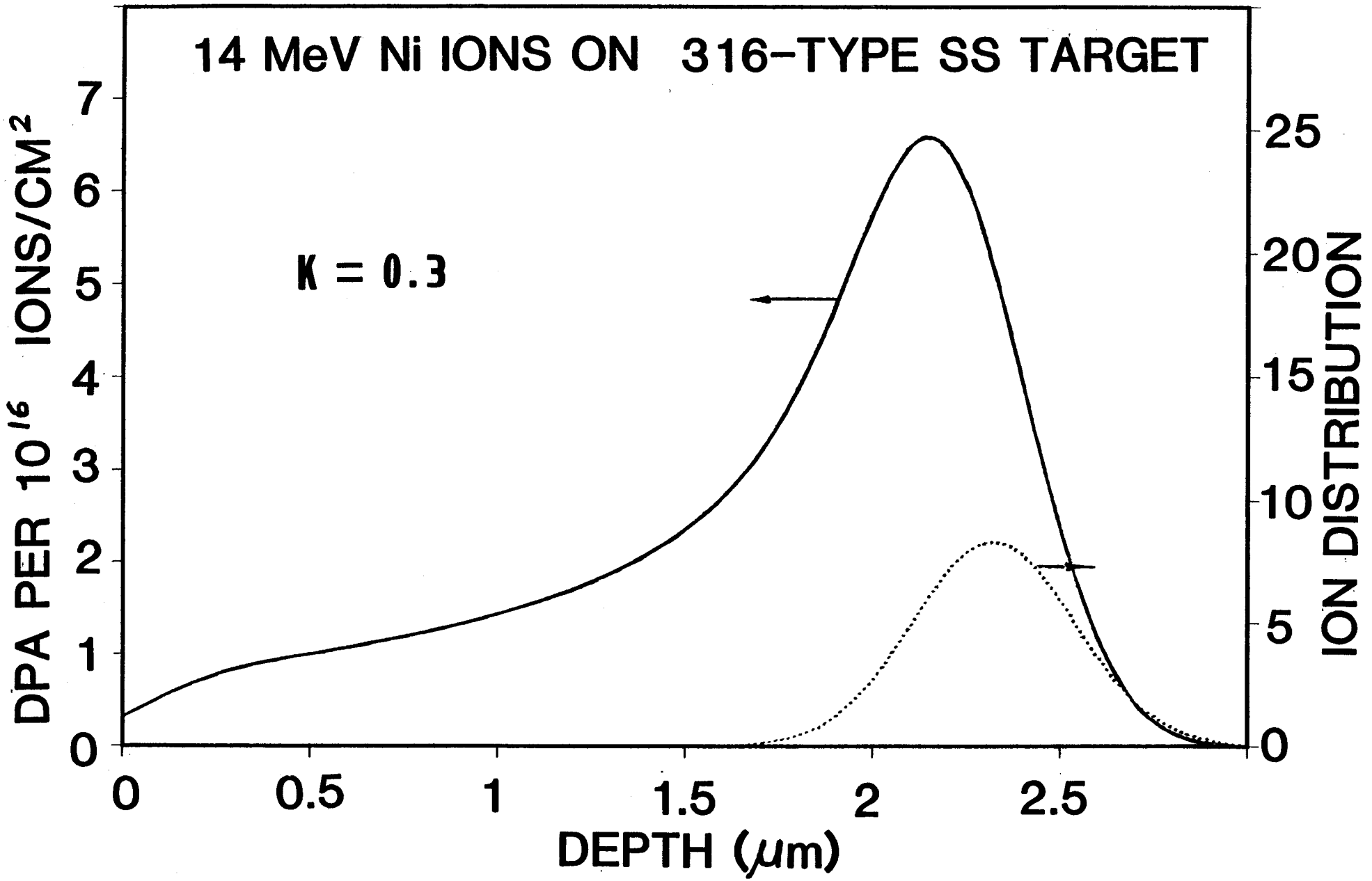
14 MeV Ni IONS ON 316-TYPE SS TARGET
K = 0.3
DPA PER 10^{16} IONS/CM^2
ION DISTRIBUTION
DEPTH (μm)
0
1
2
3
4
5
6
7
0
5
10
15
20
25
0
0.5
1
1.5
2
2.5

FIGURE 2

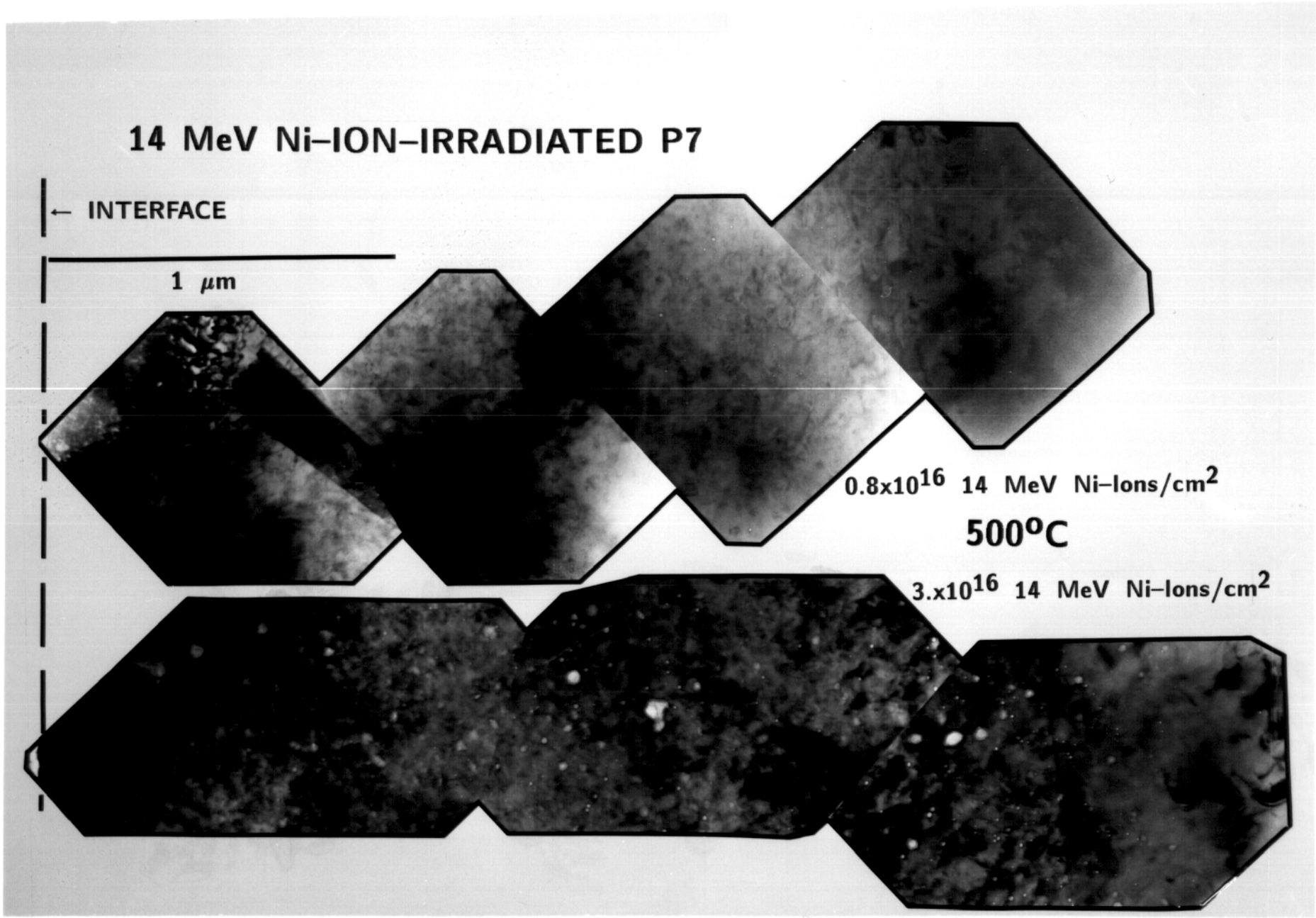
14 MeV Ni–ION–IRRADIATED P7
← INTERFACE
1 μm
0.8x10^16 14 MeV Ni–Ions/cm^2
500°C
3.x10^16 14 MeV Ni–Ions/cm^2

FIGURE 3

VOID PARAMETERS IN IRRADIATED P7 ALLOY

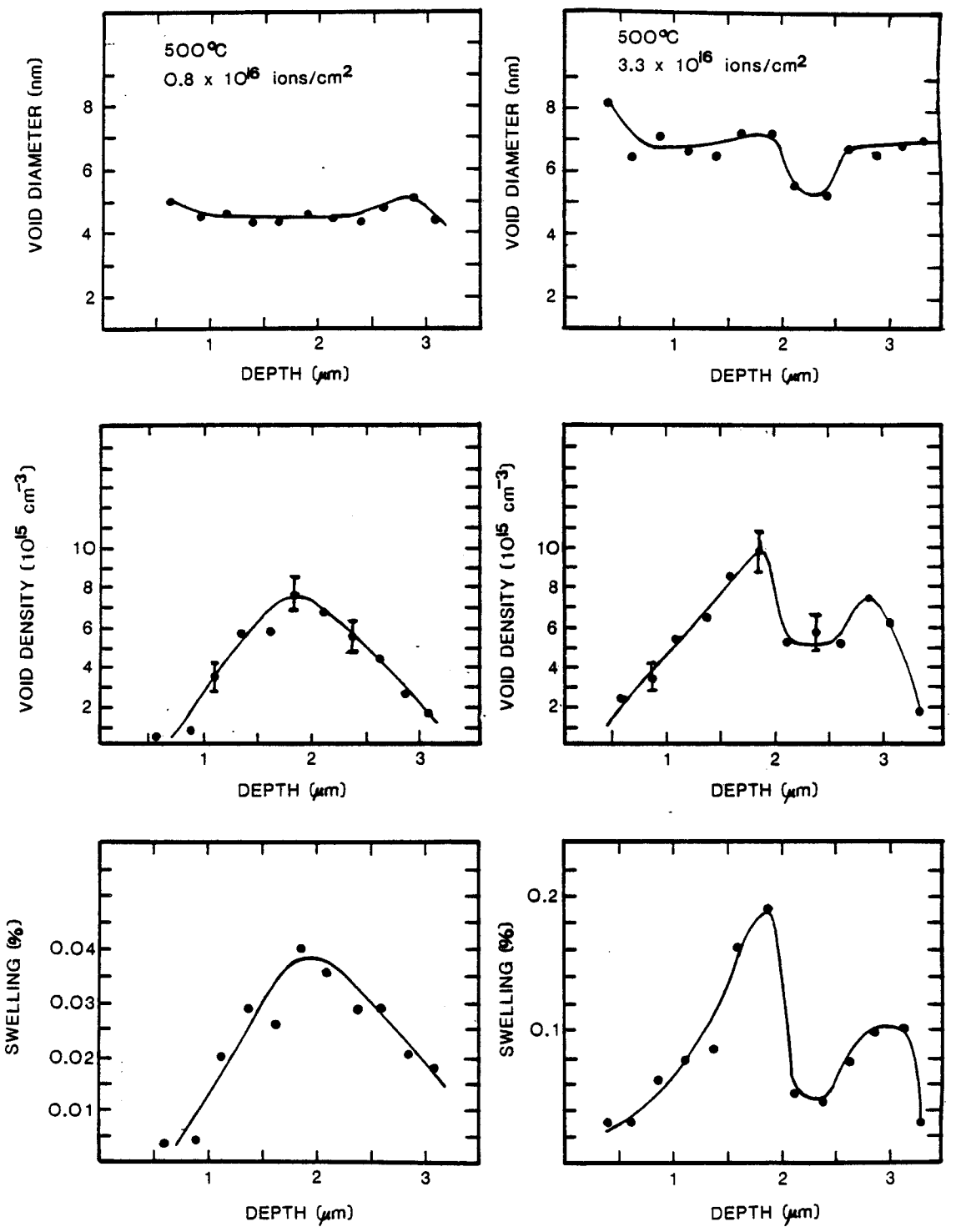

FIGURE 4

DEVELOPMENT OF THE BIMODAL VOID DISTRIBUTION IN THE P7 ALLOY

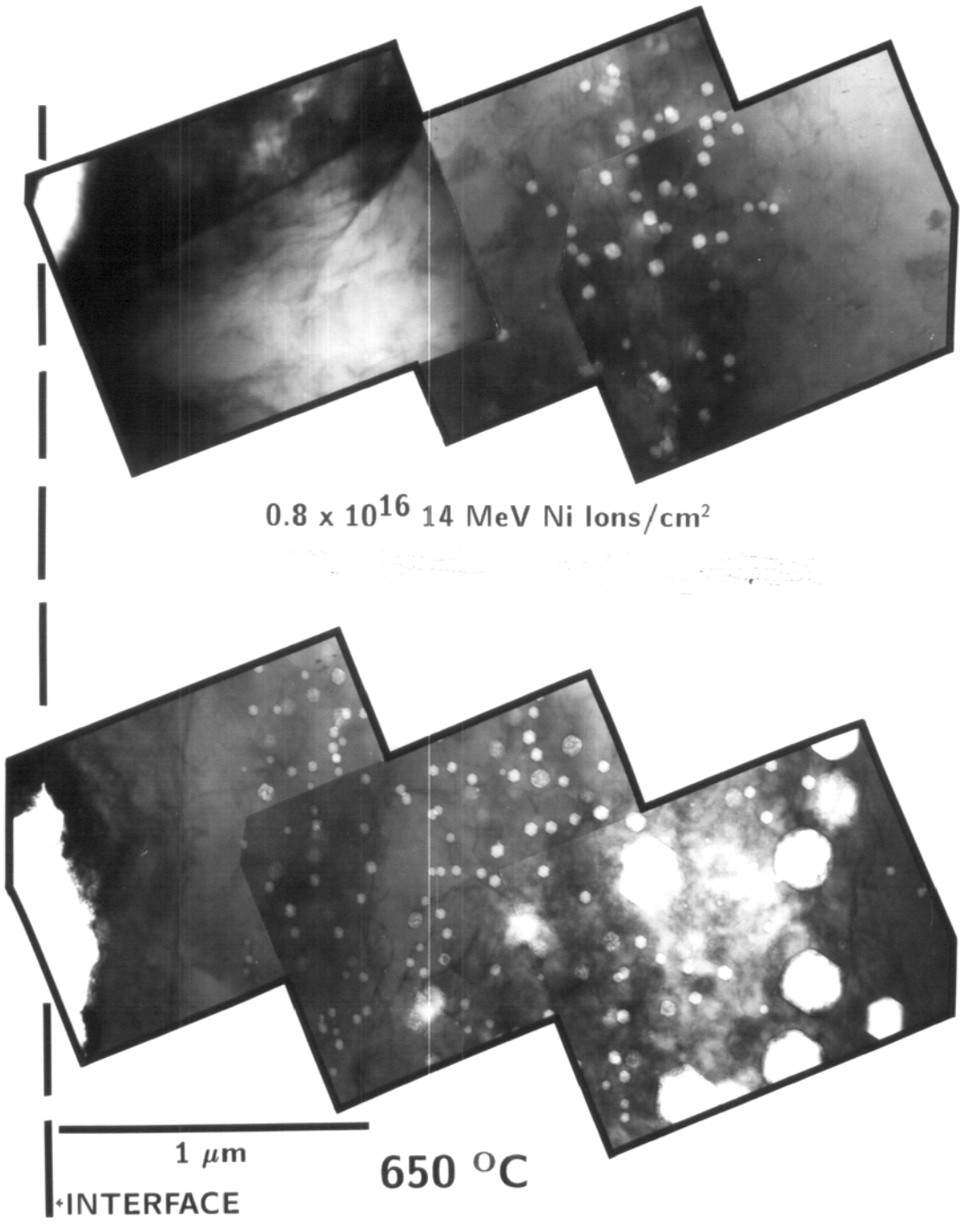

FIGURE 5

VOID PARAMETERS IN IRRADIATED P7 ALLOY

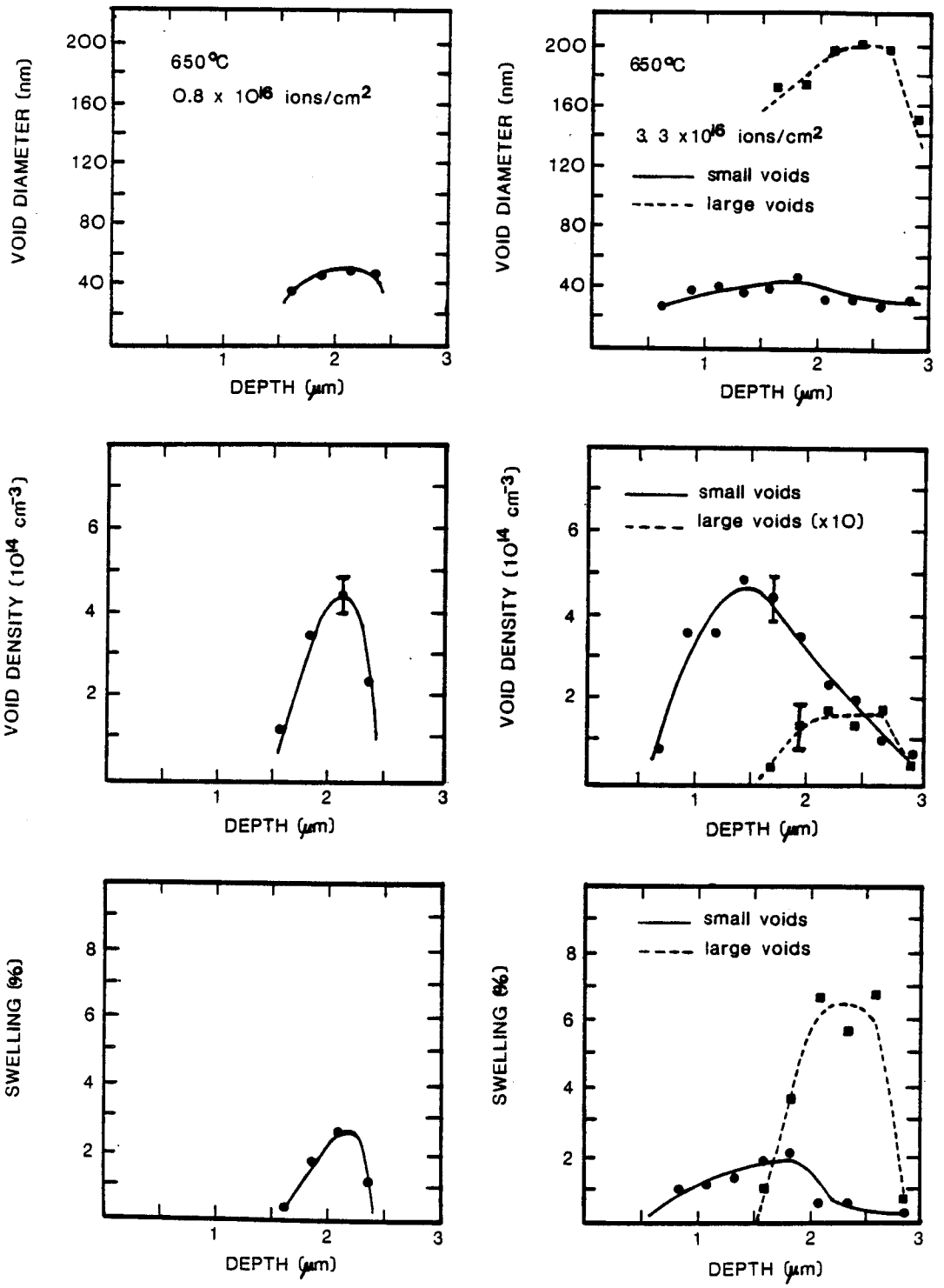

FIGURE 6

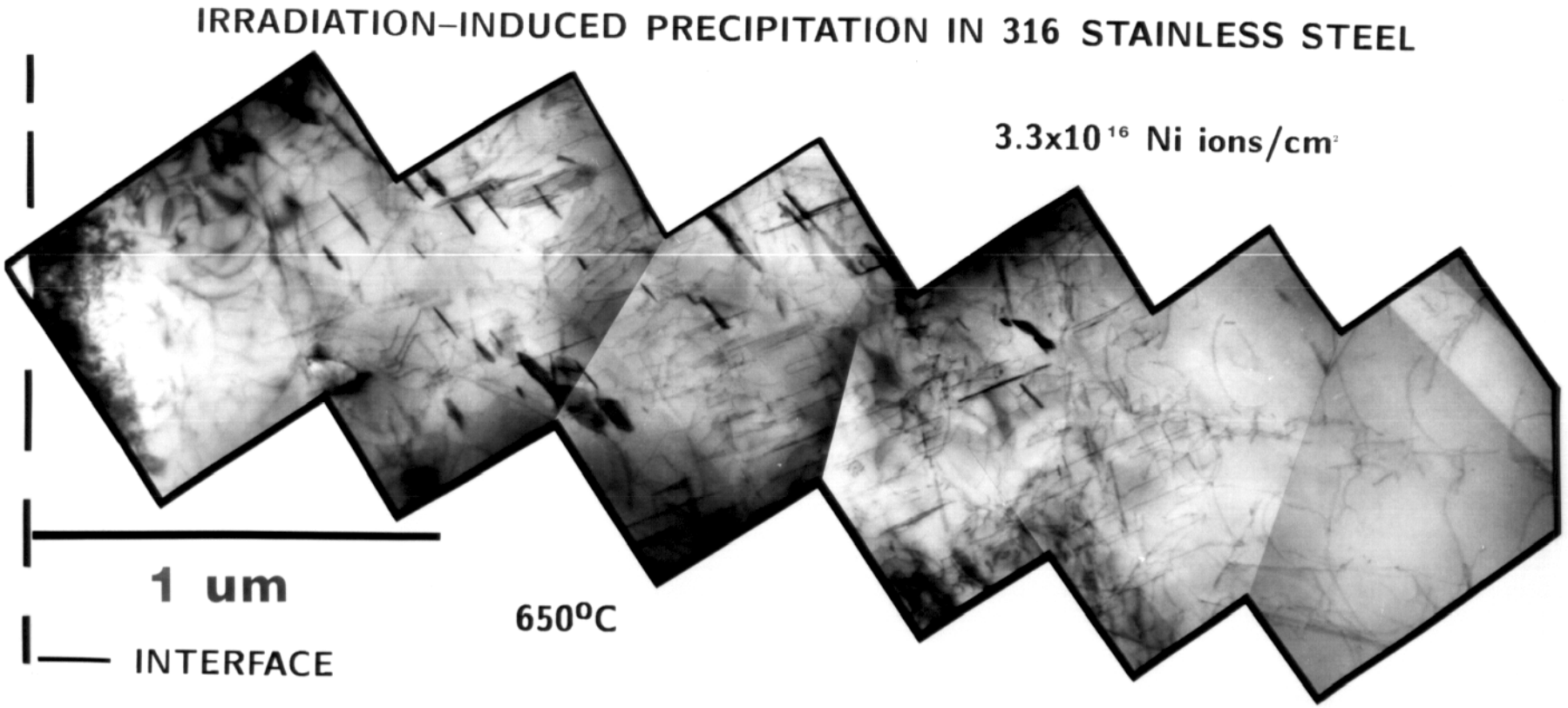
IRRADIATION–INDUCED PRECIPITATION IN 316 STAINLESS STEEL
3.3x10 16 Ni ions/cm2
1 um
650°C
INTERFACE

FIGURE 7